Volume 27
Number 34
14 September 2025
Pages 17617–18040

PCCP

Physical Chemistry Chemical Physics

rsc.li/pccp

25 YEARS ANNIVERSARY

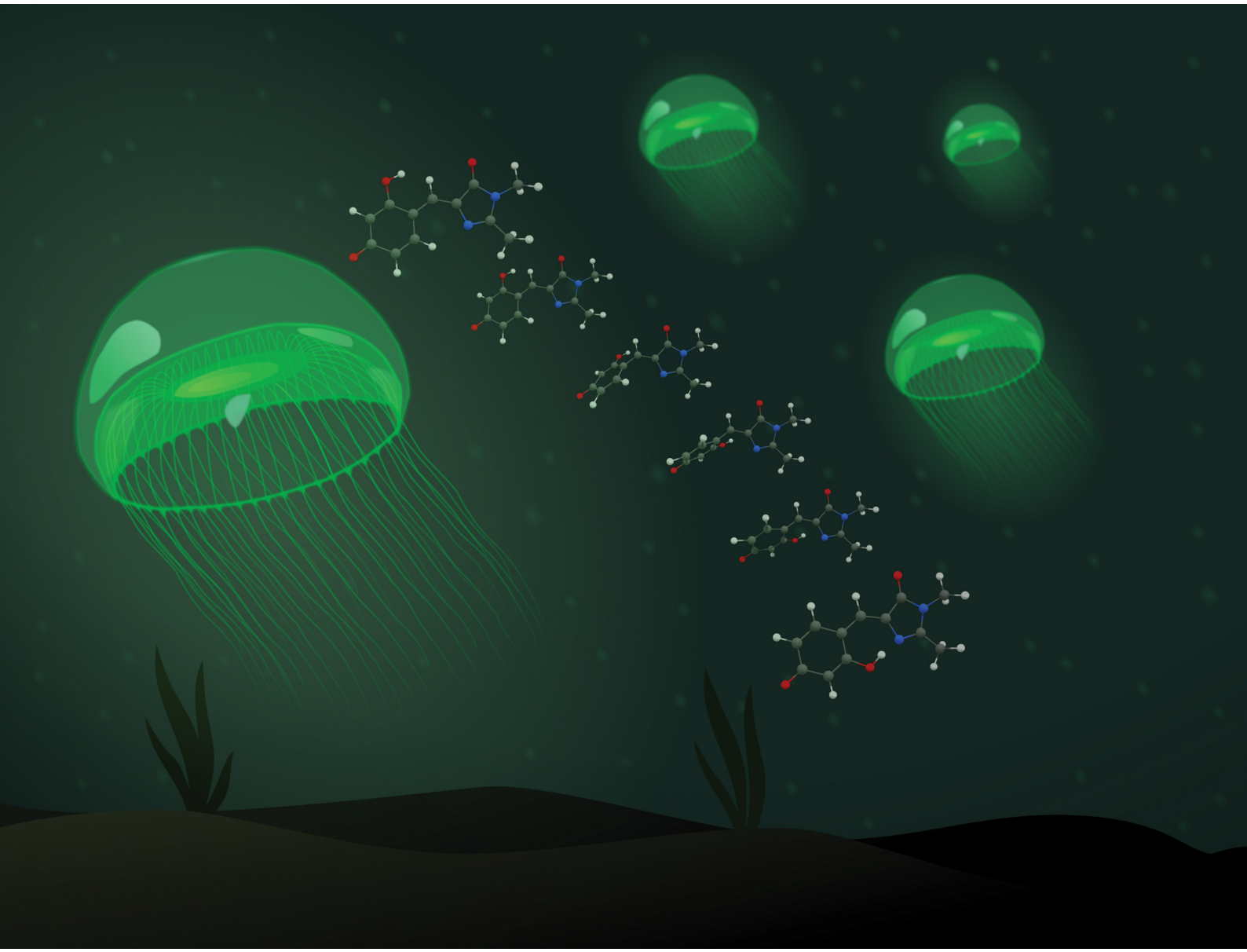

ISSN 1463-9076

ROYAL SOCIETY OF CHEMISTRY

PAPER

L. H. Andersen *et al.*

Conformer specific photophysical properties of an analog of the green fluorescent protein chromophore anion

PCCP Owner Societies

PCCP

ROYAL SOCIETY OF CHEMISTRY

PAPER

View Article Online
View Journal | View Issue

Cite this: *Phys. Chem. Chem. Phys.*, 2025, **27**, 17686

Conformer specific photophysical properties of an analog of the green fluorescent protein chromophore anion†

A. G. S. Lauridsen, A. P. Rasmussen, N. Klinkby and L. H. Andersen *

We present a spectroscopic study of a cryogenically cooled GFP chromophore derivative with an additional OH group attached to the phenol ring at the *ortho* position. Using a depletion technique, we decomposed the spectrum and identified the presence of two conformers. The absorption maximum of one conformer, the *para-trans* form, which resembles the native GFP chromophore, has a band origin at 482.8 nm, slightly red-shifted compared to the native chromophore. In contrast, the other conformer, the *para-cis* form, features a structure where the two rings of the chromophore are locked, resulting in a significantly higher excitation energy and a corresponding 14.4 nm blue shift. Comparisons with *ab initio* TDDFT calculations reveal that low-energy modes in the excited state significantly influence the spectral absorption profiles. For the *para-trans* form, the addition of the OH group increases the intrinsic energy barrier for internal conversion in the S_1 state from 250 cm^{-1} (as observed for the native chromophore) to 390 cm^{-1}. This leads to an exceptionally long excited-state lifetime, which potentially may yield a high fluorescence-quantum yield. In contrast, for the *para-cis* conformer, an excited-state lifetime of 430 fs is measured, with internal conversion remaining a competing decay channel across the spectral range examined. Importantly, the OH–N ring locking in the electronic ground state of the *para-cis* isomer does not prevent internal conversion from de-activating fluorescence in the S_1 excited state.

Received 24th June 2025,
Accepted 25th July 2025

DOI: 10.1039/d5cp02407b

rsc.li/pccp

1. Introduction

The green fluorescent protein (GFP) was first discovered in the jellyfish Aequorea victoria by Shimomura *et al.* in 1961[1,2] and has later found widespread use as a biomarker.[3–5] The fluorescence from GFP is ascribed to the anionic form of its chromophore, which is buried within an 11-stranded β-barrel structure.[2] This structure enables fluorescence with high quantum yield,[3] whereas outside the protein environment, the fluorescence of the chromophore is lost at room temperature.

Recently, spectroscopic[6] and excited-state dynamics[7] measurements of a cryogenically cooled GFP chromophore model, *p*-HBDI (4-hydroxybenzylidene-1,2-dimethylimidazolinone) anion *in vacuo*, revealed a $\sim$ 250 cm^{-1} energy barrier towards internal conversion (IC) in the bright first excited state (S_1).[6,8] Since IC is hindered by this barrier, the vibrational ground state in S_1 decays slowly, with a lifetime of 5.2 $\pm$ 0.3 ns.[7] Internal conversion and fluorescence are two competing decay channels from electronically excited states, and the long life time provides indirect evidence of fluorescence, suggesting that fluorescence is an intrinsic property of the isolated *p*-$HBDI^-$ chromophore at cryogenic temperatures. Indeed, upon photoexcitation near the band origin, fluorescence from the native *p*-HBDI anion *in vacuo* was recently detected at a temperature where some population remained behind the 250 cm^{-1} energy barrier in S_1, preventing rapid radiationless IC to the S_0 ground state.[9]

Much effort has been put into modifying *p*-HBDI, to diminish the IC-induced quenching of the fluorescence outside the protein environment. As the pathway to IC for *p*-$HBDI^-$ involves rotation around the central C–C–C methine bridge,[8] many derivatives of the GFP chromophore with this rotation hindered have been considered. Modifications of the *p*-HBDI that lock the rotation around the C–C–C methine bridge, could involve bond formation between the two rings.[10–12] It might also involve an electron-donating modification to the phenolate ring which, due to the charge transfer nature of the twisting motion,[13–15] hinders the rotation.[16] Some modifications have successfully been found to have high fluorescence quantum yield in solution.[17,18]

As mentioned, fluorescence and IC are two competing decay channels from the photoexcited bright S_1 state and since thermally induced statistical electron emission in the hot ground state (thermionic emission; TE) may happen after IC,

Department of Physics and Astronomy, Aarhus University, DK-8000 Aarhus C, Denmark. E-mail: LHA@phys.au.dk; Tel: +45 23382033

† Electronic supplementary information (ESI) available. See DOI: https://doi.org/10.1039/d5cp02407b

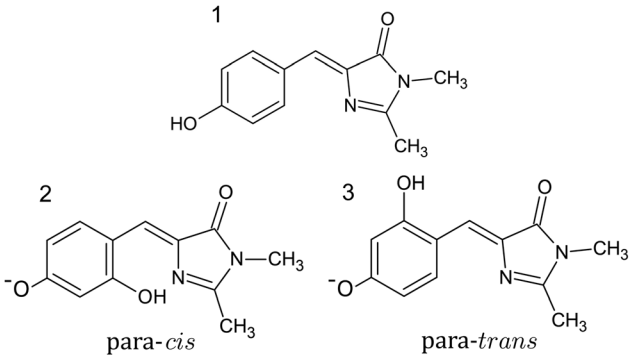

Fig. 1 (1) Neutral form of a model for the native GFP chromophore (*p*-HBDI). (2) The lowest-energy conformer of the deprotonated *op*-DHBDI$^-$ anion named the *para-cis* conformer. (3) The deprotonated *op*-DHBDI$^-$ anion named the *para-trans* conformer. The molecules are in the present studies considered under vacuum conditions (*i.e.* in gas phase).

the lack of TE might be taken as a sign that the chromophore is fluorescent. This was explored in an electron-emission study of three GFP-model chromophores,[19] where it was found that the formation of a seven membered ring structure between the imidazolino ring and the phenol ring in the *op*-DHBDI$^-$ chromophore (see Fig. 1 and 2) supresses TE, without significantly changing the spectroscopy, except for a slight blue shift.

In this work, we investigate the photophysical properties (spectroscopy and excited-state lifetime) of the deprotonated (anionic) form of *op*-DHBDI$^-$ (2,4-dihydroxybenzylidene-1,2-dimethylimidazolinone), a modified structural analogue of the GFP chromophore *p*-HBDI (see Fig. 1). Through cryogenic cooling, we resolve two distinct conformers and unveil their unique excited-state behaviors. One conformer mirrors the photophysics of the native GFP chromophore, while the other exhibits a blue-shifted spectrum and a markedly shorter excited-state lifetime. Additionally, the vibrational features reveal differences between the two conformers in the low-energy modes. The experimental results are supported by high-level *ab initio* quantum-chemistry calculations, offering deeper insight into the molecular basis of their divergent photophysical properties. Through this study we explore the relationship between chromophore conformation and photophysical behavior, with potential implications for understanding and designing fluorescent proteins and related compounds.

2. Experiment

The measurements were performed at the ion-storage ring SAPHIRA[6,7,21,22] (see Fig. 2a). An electrospray ionization-ion source was used to bring *op*-DHBDI$^-$ to the gas phase. The ions were first accumulated in a 16-pole radio-frequency (RF) ion trap, before being accelerated to 4 keV. Once accelerated, the ions were mass-to-charge selected in a magnetic field. The ions were then decelerated and trapped in another 16-pole RF-ion trap cooled to 6 K.[22] In the cold trap, the ions were stored for a duration between 150 ms and 190 ms while being cooled by He-buffer gas. After cooling, the ions were accelerated back to 4 keV and guided into SAPHIRA. The ring was kept at room temperature and at a pressure of about 3×10^{-9} mbar. The ions were allowed to circulate for a few revolutions, with a revolution time of about 60 μs (see Fig. 2b(i)) before being irradiated by laser light, in a straight section of the ring. Neutral fragments were detected by a ''prompt'' microchannel plate (MCP) detector mounted directly after the straight section of the ring in which the ions were irradiated. The prompt MCP detector had a central hole to allow the laser light to pass through. Behind the detector, the laser-pulse energy was recorded by a power meter. The photo-induced neutral fragments detected by the prompt MCP just after irradiation constitute the prompt action signal. An additional ''delayed'' MCP was located behind another arm of the ring (Fig. 2a), detecting delayed action from tens of microseconds to milliseconds after excitation (Fig. 2b(i)).

The number of photo-induced neutral fragments (Fig. 2b(i)) as a function of wavelength constitutes the action-absorption signal. The signal was normalized to the number of photons in the laser pulse and the number of ions in the ring. Importantly, relaxation pathways that do not lead to the production of neutral particles do not contribute to the action-absorption spectrum.[23] The spectrum of the *op*-DHBDI$^-$ was measured by irradiating the ions with nanosecond-laser pulses of adjustable photon energy generated by an EKSPLA NT232-50-SH-SFG (absorption laser, Fig. 2a).

A hole-burning technique was employed to demonstrate that the recorded spectrum included contributions from multiple conformers. Nanosecond laser pulses were generated using an EKSPLA NT342-3-C-UVE laser system (referred to as the depletion laser; see Fig. 2a) and directed into the cryogenic RF ion trap during the 190 ms ion cooling period. After sufficient cooling, the conformers exhibited non-overlapping absorption profiles, allowing selective depletion of a single conformer *via* interaction with the depletion laser. To facilitate differential measurements, a chopper wheel was employed to block the depletion laser on every second cycle of the experiment, enabling the simultaneous acquisition of spectra with and without photodepletion of the ions. Time gating of the ion injection into the storage ring was implemented to prevent unwanted charged photofragments generated during the depletion process from being stored. Additionally, Fourier analysis of the stored ion beam confirmed the absence of such photofragments in the ring (see ESI†).

To measure the temporal evolution of the electronically excited state, a pump–probe scheme was used.[8] Femtosecond-laser pulses were generated by a Coherent Libra UFS-HFS (named the lifetime laser, Fig. 2a), and split into two beams designated the pump and probe beam, respectively. The 800 nm probe beam was guided through a variable delay stage, allowing control of the temporal delay between the pump and probe pulses. The pump pulse was guided through a tunable optical parametric amplifier system (light conversion TOPAS) to allow control of the pump-photon wavelength. Further control of the spectral properties of the pump pulse was achieved using a pulse shaper.[7] This allowed the spectral profile of the pump pulses to be narrowed, at the expense of making the pulses

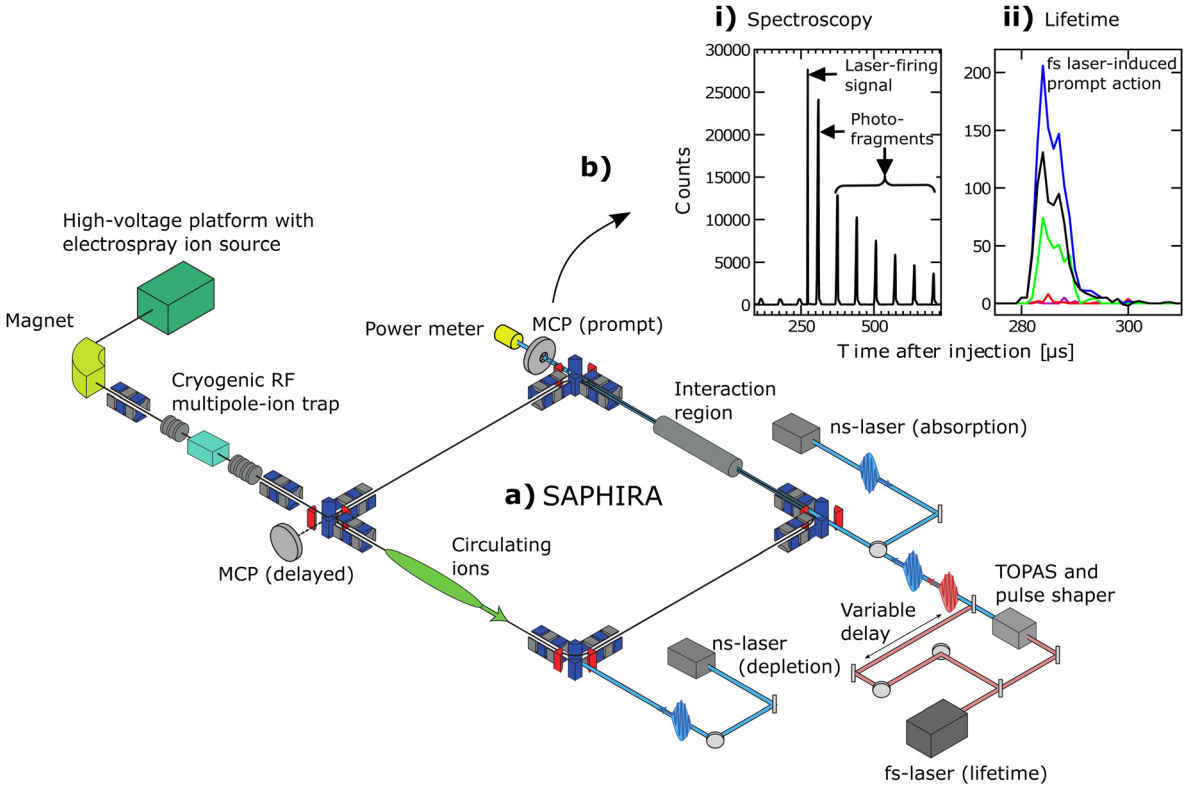

Fig. 2 (a) The ion-storage ring SAPHIRA including ion source, detectors, and laser systems shown schematically. (b(i)) Histogram of the number of neutral particles on the delayed MCP detector as a function of time after injection in the spectroscopy experiment. A sharp signal on the detector shows the moment where the laser is fired. (b(ii)) Histogram of the number of neutral particles on the prompt-MCP detector as a function of time after injection in the excited state lifetime measurement. This inset shows the peak immediately after fs-laser irradiation with the following laser-pulse combinations: pump and probe (blue), probe alone (green), pump alone (red), no laser pulse (magenta). The black curve is the resulting signal after background and single-pulse subtrafor detction, used in the fs-pump–probe lifetime measurements.

temporally longer. Different regimes of the absorption profile were addressed by the spectrally narrowed pulses. The cross-correlation between the pump and probe pulses was measured to ensure that it was short compared to the lifetimes measured. The setup for measuring the cross-correlation and the method used for simultaneous fitting the lifetimes and the cross-correlation is described in the ESI.†

3. Results

Two distinctly different regions are seen in the action-absorption spectrum of *op*-DHBDI$^-$ (Fig. 3). Below about 21 400 cm^{-1} the action peaks are narrow and low in yield while above they are wide and have higher yield. Based on TDDFT quantum-chemistry calculations the two regions of absorption are assigned to two different conformers, with the region below 21 400 cm^{-1} attributed to the *para-trans* conformer and the region above attributed mainly to the *para-cis* conformer.

The hole-burning technique confirmed that the spectrum contained signal from two conformers. The depletion laser irradiated the ions inside the RF-ion trap with photons of energy 20 747 cm^{-1} corresponding to the second peak attributed to the *para-trans* conformer. The hole-burning spectrum (Fig. 4) clearly shows that peaks attributed to the *para-cis* conformer are not affected by the depletion, whereas the heights of peaks attributed to the *para-trans* conformer are reduced.

Considering the action-absorption spectrum of the *para-cis* conformer (Fig. 3), it is seen that the delayed and prompt spectra are, up to a scaling, almost identical. The vertical photodetachment energy of *op*-DHBDI$^-$ is 23 390 cm^{-1} (428 nm).[19] Thus, resonances in the spectral region addressed here are all below this energy and not subject to autodetachment. The delayed signal is attributed to IC in the first excited state followed by statistical fragmentation in the ground state, with the signal growing approximately linearly with laser power (see ESI†). The prompt signal is attributed to one-color resonant enhanced multi-photon electron detachment (REMPD) as well as fast statistical fragmentation in the (hot) ground state after sequential multi-photon absorption.[24] The prompt signal grows approximately with the square of the laser power (see ESI†).

The first broad peak of the *para-cis* conformer appears at about 21 440 cm^{-1}. Since the delayed and prompt signals both exhibit this peak, there is no, or only a small, barrier for IC from S_1 to S_0 for the *para-cis op*-DHBDI$^-$ conformer. Rotation around the imidazolinone ring angle leads to a conical intersection

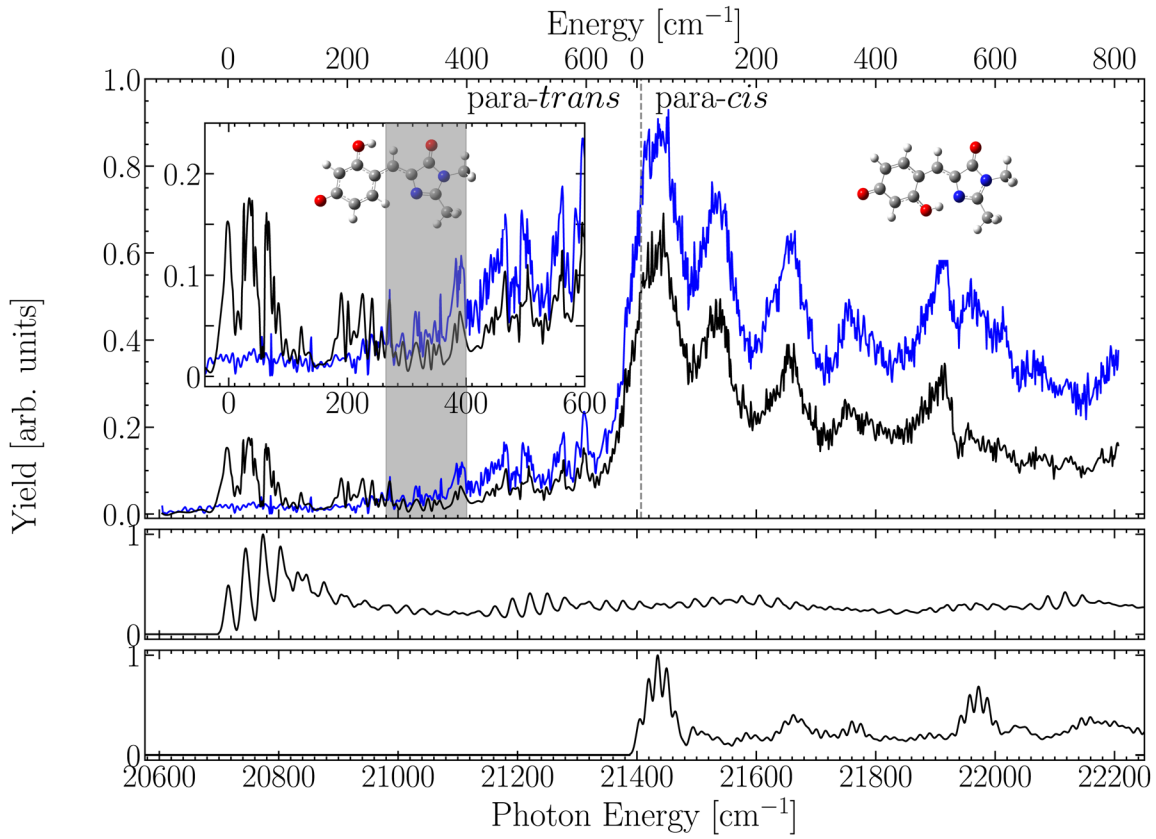

Fig. 3 Vibrationally resolved (S_1) action-absorption spectrum of the *op*-DHBDI$^-$ anion (analyzed with a cubic-spline smoothing factor of 0.2 for clarity). The prompt spectrum is shown in black and the delayed spectrum in blue. Peaks below 21 400 cm^{-1} (indicated by the dashed line) are attributed to the *para-trans* conformer (Fig. 1(3)) while the peaks above 21 400 cm^{-1} are attributed mainly to the *para-cis* conformer. The grey shaded area indicates the region of the barrier to internal conversion in the *para-trans* conformer. Delayed action vanishes below this region while prompt as well as delayed IC-based action appear above it. On the secondary top axis, energy is relative to the estimated band origin for *para-trans* and *para-cis* conformers, at 20 713 ± 10 cm^{-1} (482.8 nm) and 21 407 ± 10 cm^{-1} (467.1 nm), respectively. The two lower panels show calculated $S_0 \rightarrow S_1$ Franck–Condon spectra of the two conformers, based on CAM-B3LYP/def2tzvp TDDFT calculations, as implemented by the Gaussian16 program package.[20] The absolute energy scale for the two calculations is adjusted to the experimental spectrum. The spectra were calculated with a temperature of 6 K and convoluted with a 5 cm^{-1} HWHM smoothing function. The inserted molecular structures are the optimized geometries in the S_1 state.

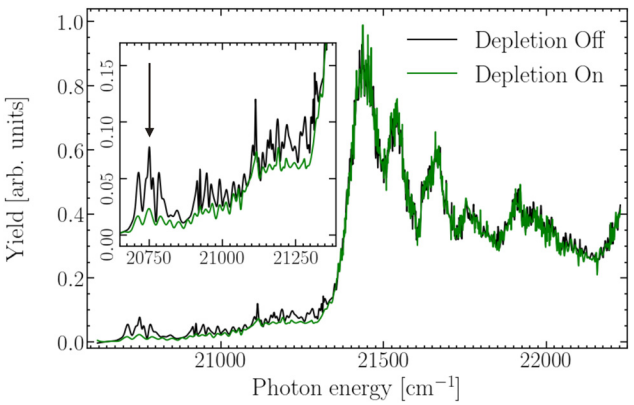

Fig. 4 Prompt action-absorption spectrum without a depletion laser (black), and with a depletion laser (green) being applied. The arrow at 20 747 cm^{-1} indicates the photon energy of the depleting photons.

which provides the pathway for IC as previously reported.[8] According to the TDDFT calculations the 0-0 band origin appears on the low-energy shoulder of the broad peak and we estimate that the band origin of the S_0–S_1 transition is at 21 407 cm^{-1} (467.1 nm). Relative to the native chromophore having a band origin at 481.5 nm,[6] the spectrum has a significant blue shift of 14.4 nm.

The action-absorption spectrum of the *para-trans* conformer shows that the threshold for delayed action appears at a higher photon energy than that of the prompt action. This indicates that a barrier for IC exists in this conformer. The first peak in the prompt action at 20 713 cm^{-1} is attributed to the band-origin of the S_0–S_1 transition of the *para-trans* conformer. Peaks in the delayed spectrum appear about 390 cm^{-1} above the band-origin, which indicates the presence of a barrier for IC for the *para-trans* conformer of about 390 cm^{-1}.

We employed time-dependent density functional theory (TDDFT) as implemented in the Gaussian16 program package[20] to optimize the *para-cis* and *para-trans* conformers in both the S_0 and S_1 electronic states and to calculate their vibrational frequencies, which are provided in the ESI.† In the ground state (S_0), the *para-cis* conformer is more stable than the *para-trans* conformer by 0.4 eV (calculated at the CAM-B3LYP/def2tzvp level of theory)

and is therefore expected to be the predominant species in the experiment. Furthermore, in the excited state (S_1), the *para-cis* conformer exhibits a relatively large dihedral twist angle of 5.6° (see ESI†), placing it closer to the conical intersection (CI) geometry. This structural feature is likely to enhance the efficiency of internal conversion and make the non-radiative deactivation channel more favorable for the *para-cis* conformer compared to the *para-trans* conformer.

The apparent difference in the Franck–Condon (FC) spectra of the *para-trans* and *para-cis* isomers, shown in Fig. 3, can be attributed to:

(i) Both isomers are planar in their electronic ground states, while in the S_1-excited state, the two rings of the chromophores adopt an angled configuration. This leads to intense excitation of a low-energy mode corresponding to this coordinate, which happens to be the lowest vibrational mode for both isomers.

(ii) The energy of this soft motion is significantly lower for the *para-cis* isomer (15 cm^{-1}) than for the *para-trans* isomer (29 cm^{-1}), leading to a smaller splitting between the harmonics of this mode in the *para-cis* isomer.

(iii) Groups of excitations involving other active modes, combined with multiple overtones of the low-energy mode, produce broad unresolved peaks, particularly for the *para-cis* isomer, due to the smaller mode energy.

The OH vibrational mode corresponding to excitation of the O–H–N bridge in the S_1 state of the *para-cis* conformer has an energy of 3023 cm^{-1} (vibr. mode number 72, see ESI†), which falls well outside the spectral range considered in this work. As a result, excited-state proton transfer is not deemed relevant here.

Three excited-state lifetime measurements were performed with different pump-pulse spectral profiles, addressing different parts of the absorption spectrum (see Fig. 5(d)). The red spectral profile addresses transitions to vibronic states below the barrier for IC in the first excited state of the *para-trans* conformer. The green spectral profile addresses transitions to vibronic states of the *para-trans* confomer above the barrier for IC. The blue spectral profile is primarily associated with states in the *para-cis* conformer. The measurement with the blue pump-pulse spectral profile (Fig. 5a) produced a lifetime of 0.43 ± 0.02 ps, consistent with fast internal conversion to S_0. Measurements with the green pump-pulse spectral profile (Fig. 5b) produced a lifetime of 94 ± 9 ps, which is comparable to the lifetime of *p*-$HBDI^-$ of a few hundred picoseconds, just above the barrier for IC.[7] Lastly, for the measurement with the red pump-pulse spectral profile (Fig. 5c) no decrease in the yield as a function of pump–probe delay was seen. Thus, the lifetimes of the vibronic states of the *para-trans* conformer below the IC barrier are at least in the nanosecond range, creating favorable conditions for fluorescence as an active decay channel.

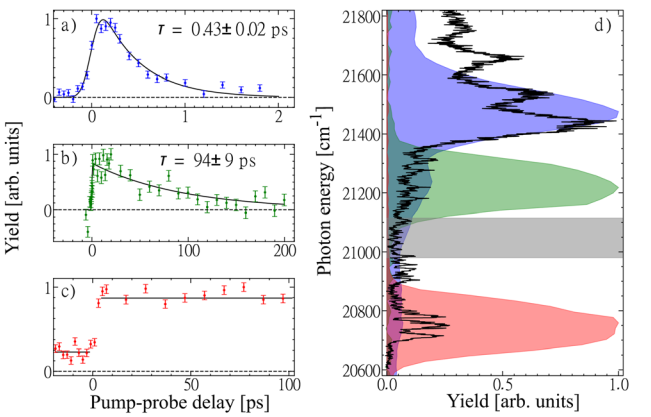

Fig. 5 Excited-state lifetimes were measured at three pump-pulse wavelengths probing different spectral regions. The excited-state decays are shown in panels (a), (b) and (c). The spectral profiles at these pump-wavelengths are seen overlaid on the prompt action-absorption spectrum in panel (d). The measured decay in a and b has been fitted to extract a lifetime. There is no measurable decay at the longest wavelength (panel (c)), and horizontal lines are to guide the eye. The grey shaded area indicates the region of the barrier to internal conversion in the *para-trans* conformer.

4. Discussion

Using action-absorption spectroscopy, the band origin of the S_0 to S_1 transition of the *para-trans* conformer of the *op*-DHBDI anion is determined to be at 20 713 cm^{-1}. This is remarkably similar to the *p*-HBDI anion, which has an S_0 to S_1 band origin of 20 768 cm^{-1}. Thus, the addition of an OH group in *para-trans op*-DHBDI changes the S_0 to S_1 transition, by only 55 cm^{-1}.

The band origin of the S_0 to S_1 transition for the *para-cis* conformer was determined to be 21 407 cm^{-1}, corresponding to a blue shift of 694 cm^{-1} (14.4 nm). The Franck–Condon spectrum for this conformer is inherently broader than that of the *para-trans* conformer, which can be attributed to significant contributions of combination bands involving low-energy distortion modes. This broadening arises from the fact that the excited states are non-planar, whereas the ground states of both isomers are planar.

The presence of an OH group plays a crucial role in modulating the excited-state dynamics, especially in terms of internal conversion and fluorescence. For the *para-trans* form, the addition of the OH group increases the intrinsic energy barrier for internal conversion from 250 cm^{-1} (native chromophore) to 390 cm^{-1}. This raised energy barrier impedes non-radiative internal conversion from the excited electronic state to the ground state. As a result of the higher barrier, the molecule remains in the excited state for a longer time, with an exceptionally long excited-state lifetime, which implies that radiative decay may become a dominant process, leading to a high fluorescence quantum yield. This shows that a small structural change to the phenolate ring of the GFP chromophore analog may enhance the fluorescence properties of the chromophore *in vacuo*, something which may be investigated in the future.[9]

For the *para-cis* form, the measured excited-state lifetime is significantly shorter, about 430 femtoseconds, which suggests that internal conversion is more prominent in this conformer. It continues to compete effectively with fluorescence across the

spectral range examined. Thus, the OH–N interaction's role in stabilizing the *para-cis* conformer in the ground state does not necessarily translate to efficient fluorescence in the excited state. Fluorescence may hence be quenched and the lifetime shortened, despite the stabilizing ring-locking mechanism in the ground state.

Conclusions

Based on this study, we conclude that although the OH–N interaction stabilizes the *para-cis* conformer in the ground state, this ring-locking mechanism does not prevent internal conversion in the excited state, which deactivates fluorescence and shortens the lifetime, which at first sight may seem counterintuitive. The *para-trans* form exhibits a long-lived excited state and potentially high fluorescence quantum yield due to an increased energy barrier for internal conversion. The OH group thus has different effects on these two isomers, potentially enhancing fluorescence in the *para-trans* but not in the *para-cis*.

Conflicts of interest

There are no conflicts to declare.

Data availability

Experimental data sets are available at the following location: **https://doi.org/10.5281/zenodo.15719453**.

Acknowledgements

We thank Mikhail S. Baranov for providing the molecules examined in the present work and Anastasia V. Bochenkova for valuable discussions. The numerical results presented in this work were obtained at the Centre for Scientific Computing, Aarhus **https://phys.au.dk/forskning/faciliteter/cscaa/**.

References

1 O. Shimomura, F. H. Johnson and Y. Saiga, *J. Cell. Comp. Physiol.*, 1962, **59**, 223–239.
2 M. Ormö, A. B. Cubitt, K. Kallio, L. A. Gross, R. Y. Tsien and S. J. Remington, *Science*, 1996, **273**, 1392–1395.
3 R. Y. Tsien, *Annu. Rev. Biochem.*, 1998, **67**, 509–544.
4 M. Zimmer, *Chem. Rev.*, 2002, **102**, 759–782.
5 A. Sun, H. Sun, G. Anwar, X. Lu and J. Yan, *Bioorg. Med. Chem. Lett.*, 2024, **98**, 129576.
6 L. H. Andersen, A. P. Rasmussen, H. B. Pedersen, O. B. Beletsan and A. V. Bochenkova, *J. Phys. Chem. Lett.*, 2023, **14**, 6395–6401.
7 A. P. Rasmusssen, H. B. Pedersen and L. H. Andersen, *Phys. Chem. Chem. Phys.*, 2023, **25**, 32868–32874.
8 A. Svendsen, H. V. Kiefer, H. B. Pedersen, A. V. Bochenkova and L. H. Andersen, *J. Am. Chem. Soc.*, 2017, **139**, 8766–8771.
9 T. T. Lindkvist, I. Djavani-Tabrizi, L. H. Andersen and S. B. Nielsen, *Phys. Rev. Lett.*, 2025, **134**, 093001.
10 S. Chatterjee and P. Karuso, *Tetrahedron Lett.*, 2016, **57**, 5197–5200.
11 S. A. Boulanger, C. Chen, I. N. Myasnyanko, M. S. Baranov and C. Fang, *J. Phys. Chem. B*, 2022, **126**, 5081–5093.
12 C. Chen, L. Zhu, S. A. Boulanger, N. S. Baleeva, I. N. Myasnyanko, M. S. Baranov and C. Fang, *J. Chem. Phys.*, 2020, **152**, 021101.
13 J. Langeland, N. W. Persen, E. Gruber, H. V. Kiefer, A. M. Kabylda, A. V. Bochenkova and L. H. Andersen, *Chem. Phys. Chem.*, 2021, **22**, 833–841.
14 S. Olsen, K. Lamothe and T. J. Martínez, *J. Am. Chem. Soc.*, 2010, **132**, 1192–1193.
15 M. E. Martin, F. Negri and M. Olivucci, *J. Am. Chem. Soc.*, 2004, **126**, 5452–5464.
16 N. H. List, C. M. Jones and T. J. Martínez, *Commun. Chem.*, 2024, **7**, 25.
17 Y.-H. Hsu, Y.-A. Chen, H.-W. Tseng, Z. Zhang, J.-Y. Shen, W.-T. Chuang, T.-C. Lin, C.-S. Lee, W.-Y. Hung, B.-C. Hong, S.-H. Liu and P.-T. Chou, *J. Am. Chem. Soc.*, 2014, **136**, 11805–11812.
18 M. S. Baranov, K. M. Solntsev, N. S. Baleeva, A. S. Mishin, S. A. Lukyanov, K. A. Lukyanov and I. V. Yampolsky, *Chem. – Eur. J.*, 2014, **20**, 13234–13241.
19 C. Mclaughlin, M. Assmann, M. A. Parkes, J. L. Woodhouse, R. Lewin, H. C. Hailes, G. A. Worth and H. H. Fielding, *Chem. Sci.*, 2017, **8**, 1621–1630.
20 M. J. Frisch, G. W. Trucks, H. B. Schlegel, G. E. Scuseria, M. A. Robb, J. R. Cheeseman, G. Scalmani, V. Barone, G. A. Petersson, H. Nakatsuji, X. Li, M. Caricato, A. V. Marenich, J. Bloino, B. G. Janesko, R. Gomperts, B. Mennucci, H. P. Hratchian, J. V. Ortiz, A. F. Izmaylov, J. L. Sonnenberg, D. Williams-Young, F. Ding, F. Lipparini, F. Egidi, J. Goings, B. Peng, A. Petrone, T. Henderson, D. Ranasinghe, V. G. Zakrzewski, J. Gao, N. Rega, G. Zheng, W. Liang, M. Hada, M. Ehara, K. Toyota, R. Fukuda, J. Hasegawa, M. Ishida, T. Nakajima, Y. Honda, O. Kitao, H. Nakai, T. Vreven, K. Throssell, J. A. Montgomery, Jr., J. E. Peralta, F. Ogliaro, M. J. Bearpark, J. J. Heyd, E. N. Brothers, K. N. Kudin, V. N. Staroverov, T. A. Keith, R. Kobayashi, J. Normand, K. Raghavachari, A. P. Rendell, J. C. Burant, S. S. Iyengar, J. Tomasi, M. Cossi, J. M. Millam, M. Klene, C. Adamo, R. Cammi, J. W. Ochterski, R. L. Martin, K. Morokuma, O. Farkas, J. B. Foresman and D. J. Fox, *Gaussian 16 Revision C.01*, 2016, Gaussian Inc., Wallingford CT.
21 H. B. Pedersen, A. Svendsen, L. S. Harbo, H. V. Kiefer, H. Kjeldsen, L. Lammich, Y. Toker and L. H. Andersen, *Rev. Sci. Instrum.*, 2015, **86**, 063107.
22 H. B. Pedersen, H. Juul, F. K. Mikkelsen, A. P. Rasmussen and L. H. Andersen, *Phys. Rev. A*, 2022, **106**, 053111.
23 A. V. Bochenkova and L. H. Andersen, *J. Phys. Chem. Lett.*, 2022, **13**, 6683–6685.
24 L. H. Andersen, H. Bluhme, S. Boye, T. J. D. Jørgensen, H. Krogh, I. B. Nielsen, S. B. Nielsen and A. Svendsen, *Phys. Chem. Chem. Phys.*, 2004, **6**, 2617–2627.